Inductive Heating for Research in Electrocatalysis: Theory, Practical Considerations, and Examples

Derek Esau,* Fabian M. Schuett, K. Liam Varvaris, Ludwig A. Kibler, Timo Jacob, and Gregory Jerkiewicz*

ABSTRACT: Inductive heating in neutral or slightly reducing gaseous atmosphere has become one of the most effective methods to thermally pretreat oxygen-sensitive monocrystalline electrodes for interfacial electrochemistry and electrocatalytic research. In this contribution, we discuss the principles and theory of inductive heating, and we explain how an alternating current passing through a coil induces a resistive current inside a conductive sample. The thermodynamics and heat transport phenomena of how the thermal energy propagates and heats the sample are then discussed. Practical considerations with examples are given about how to best utilize this technique and avoid sample damage by controlling the gaseous atmosphere surrounding the sample being treated. Finally, a Ni(111) electrode is used to demonstrate the applicability of the method to interfacial electrochemistry and electrocatalysis research. The post-thermal treatment demonstrates the effect of the presence of small amounts of oxygen in the gaseous atmosphere on cyclic voltammetry profiles acquired in aqueous alkaline media.

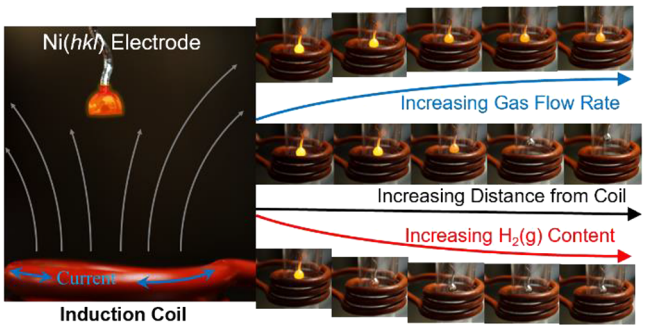

KEYWORDS: *Inductive annealing, electromagnetism, thermodynamics, heat transport, electrocatalysis, interfacial electrochemistry, single crystals, nickel electrodes*

INTRODUCTION

Research using monocrystalline surfaces has been a hallmark of electrochemical and electrocatalytic research for the past few decades. This is due in part to the fact that polycrystalline materials have complex surface structures consisting of randomly oriented monocrystalline grains and grain boundaries. Consequently, the structure of polycrystalline materials is poorly defined and is dependent on the nature of the materials and their fabrication procedures. Using clean, well-ordered, monocrystalline surfaces provides a controlled electrochemical interface where the arrangement of atoms is known or can be determined using surface analytical techniques. This greatly simplifies the determination of surface-geometry-specific thermodynamic and kinetic parameters, and the elucidation of reaction mechanisms for electrochemical processes.[1] This fundamental information is vital for better utilization of metals for heterogeneous (electro)catalysis. Conducting electrochemical measurements on monocrystalline electrode surfaces is inherently more challenging than working with polycrystalline materials. This is due to the requirement that the surface atoms must be ordered, and their arrangement must be maintained long enough for a measurement to be conducted. This is compounded by the risk of contaminating the surface, which further complicates the measurement, especially when the electrode surface pretreatment manipulations must be conducted in a separate environment or a reaction cell and then be transferred to the electrochemical cell for measurements. As a result, researchers have devised several methodologies to perform accurate measurements on clean, well-ordered monocrystalline surfaces. Ideally, one would like to prepare monocrystalline electrodes in ultrahigh vacuum (UHV) systems, which would be free of reactive gases (such as oxygen and carbon dioxide) and airborne contaminants.[2,3] However, this is unrealistic for many interfacial electrochemistry and electrocatalysis laboratories, because the cost of acquiring, running, and maintaining UHV systems is very high, and there are additional experimental challenges associated with working under UHV conditions. In addition, there are no commercial UHV-electrochemistry instruments available, and the few existing ones are designed in-house and have different configurations.[4] As a result, integrated UHV-

electrochemistry systems are rare, and most experimentalists choose to work under ambient conditions. Another complicating factor is the fact that transfer from a surface-analysis chamber to an electrochemistry chamber of UHV-electrochemistry instruments is prone to contamination.

There are two main approaches that are commonly employed to achieve atomically ordered surfaces: (electro)-chemical and thermal-based methodologies. The primary technique used to prepare surfaces using electrochemical means is by conducting controlled dissolution of the surface; this is more commonly referred to as "electropolishing".[5,6] The main idea behind electropolishing is that rougher sections of the electrode surface are more prone to dissolution than the more ordered, flatter sections, resulting in a mirror-like surface. Electropolishing is the simplest method to prepare a monocrystalline surface because no additional equipment or experimental setups are required other than an electrolyte and a potentiostat or a power supply. It is common knowledge that the surfaces that are produced using electropolishing are not as well ordered as those prepared using thermal approaches.[7,8] This is because when the rougher parts of the surface undergo preferential dissolution, dissolution is also occurring on the atomically flat terraces, leading to a certain amount of roughening in these areas. However, it is important to recognize that electropolishing is an important technique for cleaning surfaces that have accidentally, or intentionally in the case of electrodeposition experiments, become contaminated with other metals or metallic species. Thermal-based approaches are the main methods used to achieve highly ordered (atomically ordered) metallic surfaces. Introduction of thermal energy allows surface atoms to diffuse across the surface to form progressively ordered structures, from small to large clusters, to large monatomic terraces where the majority of the electrode surface is ordered. Time, temperature, and ambient conditions required to achieve a highly ordered surface are dependent on the metal being studied. Using furnaces with or without atmosphere control is perhaps the simplest means of doing this and this practice has been used for many years. However, furnaces can be quite expensive, and there are several experimental challenges associated with the transfer a single crystal from a furnace to an electrochemical cell, which can introduce surface contamination or cause surface oxidation.

The work of Clavilier et al. was ground-breaking to the field of single crystal electrochemistry as the so-called "flame annealing" technique allowed for the growth and final treatment of platinum single crystals using only a flame on a benchtop, without the requirement of furnaces or UHV equipment.[9−11] This methodology was later applied to other noble metallic electrodes and has allowed the study of monocrystalline electrode surfaces to become more attainable for many researchers. The drawback of the methodology of Clavilier et al. is that the surfaces being studied must be noble enough not to thermally oxidize in the presence of ambient oxygen present in air. Protecting the surface by cooling in an atmosphere of CO(g) or I_2(g) (vapor) and electrochemically removing these adsorbed species by oxidative desorption and reductive desorption, respectively, has proven to be an effective method of preparing some oxygen-sensitive metallic surfaces.[12] However, this is not applicable to all metals, as some metals will electrochemically oxidize or disorder before the onset of CO_{ads} stripping (oxidative desorption).[13] Cuesta et al. proposed a unique methodology that used resistive heating, by applying a high current to a single crystal that was successfully applied to research on Pd(*hkl*) electrodes. The innate electrical resistance of the sample and the high current passing through it will cause the Pd(*hkl*) electrode to heat up and will result in atomically ordered surfaces.[14] The advantage of this design was that the Pd(*hkl*) electrode could be thermally pretreated inside an electrochemical cell, without the need to transfer it from one cell to another, thus removing the risk of accidental oxidation. The drawback of resistive heating is that it requires connecting wires (typically through spot-welding) that supply the current to the single crystal. The wires must be made from the same metal as the crystal to avoid metallic contamination, and this is not feasible for all metals, metallic alloys, or thin-film deposits. Furthermore, sublimation of metals at the glowing wires carrying significant currents and redeposition on the single crystal surface may cause undesired structural modification. These obstacles were overcome with the first application of inductive heating to single-crystal electrochemical research in the Kolb Laboratory at Ulm University. The essential technique was developed by Kibler et al. and involved the annealing of single crystals in a quartz tube by an induction coil under an inert or reducing atmosphere to prevent surface oxidation. It was first applied to surface preparation and electrochemical studies of Au and Pt surfaces to validate the method and then applied to oxidation-susceptible electrode surfaces, such as Ru(0001),[15] Pd(111),[16] Ag(111) and Ag(100),[17] Ir(111),[18] Ir(210),[19] and, later, also to single-crystal alloys, e.g. Pt_xRu_{1-x}(111) electrodes.[20,21] Soon afterward, inductive heating was adopted by several interfacial electrochemistry groups and was used for the final surface preparation of noble and non-noble metals, and alloyed single crystals.[18,22−25] High-frequency generators for inductive heating were also used for the more-sophisticated designs of electrochemical cells.[26]

Interestingly, inductive heating is not yet described in detail in interfacial electrochemistry and electrocatalysis literature, and has often been viewed as a simple technique. Although it is robust and relatively simple to use while allowing contactless heating and annealing of metallic materials, there are important nuances that should be understood to best utilize the method. The present contribution outlines the theory behind inductive heating and the phenomena that result in materials being heated. It also discusses important aspects of temperature-related effects and how they influence the physical properties of materials. Lastly, practical and experimental considerations are discussed that combine theoretical and experimental observations. The method has been successfully applied and optimized in our laboratories; here, we present results for cut-and-polished, hemispherical Ni single crystals as model samples. They require lower temperatures, thus weaker magnetic fields, for heating and, consequently, are easier to image with a digital camera than, for instance, Pt single crystals. We also summarize the preparation of Ni single crystals and present cyclic voltammetry profiles for Ni(111) electrodes to demonstrate that the induction heating preserves the metallic surface and atomic arrangement of atoms.[25,27−30]

EXPERIMENTAL SECTION

The Ni single crystals that are described in this contribution were grown starting with a 1.00 mm Ni wire (Alfa Aesar, Puratronic grade, 99.999% purity) using the controlled-atmosphere flame fusion (CAFF) methodology, a detailed description of which is available elsewhere.[25,30] The procedure

for growing spherical single crystals from a wire, properly orienting, cutting, polishing, and performing the final thermal treatment is also available elsewhere.[27−29] The gases that were used were ultrahigh purity Ar(g) and H_2(g) (Praxair, 5.0 purity), and the gas flow rates were controlled with flow meters (Omega). The induction heating system used was an Ambrell EasyHeat with a three-loop induction coil with an inside diameter of 2.00 cm. During heating, the single crystals were held in place with a ceramic tube (yttria-stabilized zirconia, OMEGATITE 450, Omega). The crystals were heated in a custom-designed quartz annealing cell, with an outside diameter of 1.75 cm to ensure that the entire annealing cell fitted inside the coil, without touching it. Glassware/quartzware was precleaned by submerging all pieces in an acidified aqueous solution of $KMnO_4$ for 48 h ($KMnO_4$, Millipore-Sigma, ACS Reagent, 99.0%; concentrated H_2SO_4, FisherScientific, ACS-Pur, 98%; and ultrahigh-purity (UHP) water prepared using a Milli-Q model Direct-8 purification system, with a resistivity of $\rho \geq 18.2$ MΩ cm). As organic compounds present in trace amounts were oxidized during cleaning, $KMnO_4$ became reduced to brown, insoluble MnO_2 that was subsequently removed with dilute Caro's acid ("Piranha Solution"), prepared using 30% v/v H_2O_2 (Fisher Scientific, ACS Reagent grade), H_2SO_4 (Fisher Scientific, ACS-Pur, 98%), and UHP water, thus in accordance with well-established cleaning procedures.[29] The pyrometer (Optris, model CT 3MH3 CF) was equipped with two red lasers for alignment of the detector. Optical images were taken with a digital camera (Sony, Model α58). The electrochemical measurements were conducted in a Pyrex three-compartment cell. A Pt mesh electrode served as a counter electrode (CE) and a reversible hydrogen electrode (RHE) was used as a reference electrode (RE). The Pt CE was separated from the WE compartment using a glass frit.[31] UHP H_2(g) was bubbled through the CE compartment, so that either the hydrogen evolution reaction (HER) or the hydrogen oxidation reaction (HOR) occurred at its surface and the Pt CE was never in the potential region, which could result in its (electro-)dissolution. Consequently, the Ni(111) electrode could never be contaminated by Pt atoms originating from the CE.[32] The working electrode (WE) assembly consisted of a Ni(111) electrode connected to a Ni wire, a stainless-steel housing, which was encapsulated in a precleaned Teflon sleeve. The wire supporting the Ni(hkl) electrode was held in the stainless-steel housing, using a stainless-steel screw. The stainless-steel housing that was in contact with the Ni wire served as an external electrical connection; it was never in contact with the electrolyte solution. The electrolyte solution was prepared by dissolving NaOH pellets (Alfa Aesar, 99.996%) in UHP water. Prior to the experiments, the electrolyte solution was degassed with UHP N_2(g) (Praxair, 5.0) to expel any remaining reactive gases (mainly O_2) originating from air. The nitrogen gas was presaturated with UHP water to ensure a constant volume (thus, a constant concentration) of the electrolyte during experiments. All measurements were conducted using a Bio-Logic model SP 150 potentiostat, controlled using proprietary software. The electrochemical cell was placed inside a custom-built Faraday cage to reduce external electrical noise. The Ni(111) electrode was stored in air and, unavoidably, developed a thin oxide layer that required reduction prior to electrochemical measurements. The single crystal was annealed in a Ar(g)/H_2(g) mixture (1:1 ratio) at 1250 °C for 10 min, using a custom-designed quartz annealing cell. Then, the Ni single crystal was slowly cooled in the same gas mixture. In order to protect the Ni(111) surface from contamination and oxidation during the transfer from the annealing cell to the electrochemical cell, it was protected with a droplet of degassed UHP water.[25,29] The single crystal protected with the UHP water droplet was carefully transferred to the electrochemical cell for measurements.

THEORY OF INDUCTIVE HEATING

In the following sections, we introduce the fundamental theory behind induction heating and the factors that contribute to how a sample is heated. This section is by no means exhaustive, and the reader is encouraged to consult the cited literature for a more complete and detailed understanding of the concepts if it is required (particularly those concerning electromagnetism). Nevertheless, we feel that the explanations given below will assist the reader in the understanding of the general usage and appreciation for the technique. It is always advisible to make use of material provided by manufacturers of induction heating systems for technical information about their systems as well as specifics associated with their designs. We begin with Ampere's Law, which states that a conductor with a current passing through it will produce a magnetic field proportional to the magnitude of the current:

$$\oint_S \vec{B}\cdot d\vec{l} = \mu_o I \tag{1}$$

where $\vec{B}$ is the magnetic field (T), $\vec{l}$ the distance vector (m), μ_o the permeability of a vacuum (T m A^{-1}), and I the applied current (A). For inductive heating, typically one is working with a circular coil or coils (although the coils that are used can often be customized to fit specific requirements), and the general expression that models the magnetic field generated by a circular loop is given by the following:

$$|\vec{B}| = \frac{N}{|\vec{l}|}\mu_o I \tag{2}$$

where B is now the magnetic field strength in the center of the coil (T) and N is the number of loops in the coil. The Biot−Savart Law allows for the strength of the magnetic field at some distance r (m) from the induction coil to be determined in the following manner:[33]

$$\vec{B}(\vec{r}) = \frac{\mu_o}{4\pi}\int I\frac{d\vec{l}\times\vec{r}}{|r|^3} \tag{3}$$

If one assumes they are working with a single loop coil (many commercial induction heaters are single loop systems) and that one desires to know the magnetic field strength in the center of the coil, which is the most practical way to heat a small sample inside a larger induction heating coil, then a practical formula can be used:[33,34]

$$B(r) = \frac{\mu_o I}{4\pi}\left[\frac{2\pi {R_{coil}}^2}{({r_c}^2 + {R_{coil}}^2)^{3/2}}\right] \tag{4}$$

with R_{coil} being assigned to the radius of the coil (m) and r_c is the distance from the center of the coil.

Plotting the outcome of eq 4, with respect to the distance from the center of the coil, as shown in Figure 1 for a coil with a radius of 10 mm and an applied alternating current of 100 A, has some important experimental consequences that should be discussed. First, the magnetic field is strongest in the center of

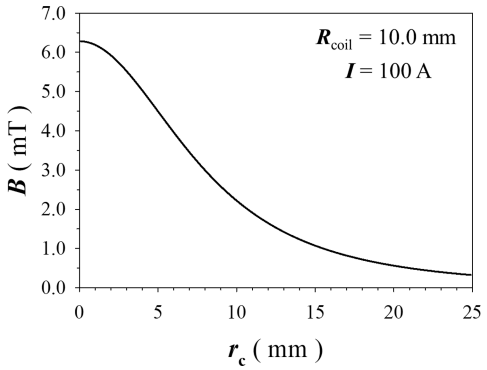

Figure 1. Plot of Ampere's Law showing the change of magnetic field strength for a single loop induction coil with a radius of 10.0 mm and an applied alternating current of 100 A.

the coil (at the origin of the circular coil and r_c = 0 mm), as shown by the small plateau as the distance from the coil approaches zero. Second, the magnetic field strength decays exponentially as one increases the distance of the sample to the coil. This property implies that there is an effective working distance, depending on several physical properties of the sample. Lastly, it is important to note how the magnetic field strength changes within the desired working distance. If one looks at the field strength at 10 mm and imagines that the sample is moved by 5 mm closer to the coil, then the magnetic field experienced by the sample effectively doubles. This implies that even slight variations in the working distance can cause large differences when heating the sample, as it will be discussed below in the section entitled "Sample Positioning". The Faraday–Lenz Law relates how a sample will interact with an external magnetic field and induces an opposing electric field (electromotive force) inside the sample:[33]

$$\varepsilon = -\frac{d\phi_B}{dt} \tag{5}$$

where ε is the induced electric field strength (electromotive force) in the sample (V) and $d\phi_B/dt$ is the change in magnetic flux (T m^2 s^{-1} or V). The negative sign in eq 5 implies that the electromotive force produced within the sample is acting opposite to the magnetic field with which the sample is interacting. The presence of an electromotive force within the sample causes the formation of circulating, so-called "eddy", currents within the sample, given by Ohm's Law:[33]

$$|\varepsilon| = V = I_p R \Leftrightarrow I_p = \frac{V}{R} \tag{6}$$

where V is the induced electromotive force in the sample (V), I_p the induced current in the sample (A), and R the resistance in the sample (Ω). The eddy currents that are induced in the sample are converted to thermal energy via the "Joule Effect", which relates current and resistance to power:[33]

$$P = I_p V \Leftrightarrow P = \frac{V^2}{R} = I_p{}^2 R \tag{7}$$

where P is the power experienced by the sample (W or J s^{-1}), which converts to thermal energy per unit of time.

The previous section about the processes involved in inductive heating of metallic samples can be summarized in the following manner and is pictured in Figure 2:

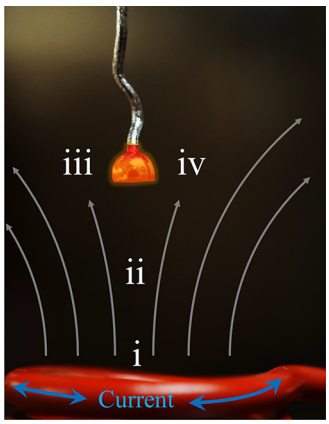

Figure 2. Diagram summarizing the elementary steps of induction heating on a cut and oriented Ni single crystal.

(i) When an alternating current is passed through a coil, a magnetic field is generated around the coil and extends into space, according to Ampere's Law;
(ii) The magnetic field indices an opposing electromotive force inside a metallic sample when the sample is placed in the center of the coil, according to the Faraday–Lenz Law;
(iii) The induced electromotive force produces circulating eddy currents inside the sample, following Ohm's Law; and
(iv) The eddy currents are then converted to thermal energy via the Joule Effect.

This section has discussed the working principles of inductive heating and how electromagnetic effects produce thermal energy inside a conductive (metallic) sample. In the following sections, we will discuss the electric and magnetic properties of the coil and the material being heated, and also the thermal properties of materials, and how they change with temperature.

ELECTRIC AND MAGNETIC CONSIDERATIONS

The ability for a material to interact with an external magnetic field is related to the magnetic permeability of the substance, given by the following relationship:[35]

$$\vec{B}(\vec{r}) = \mu\vec{H}(\vec{r}) = \mu_o\mu_r\vec{H}(\vec{r}) \tag{8}$$

In this relationship, $\vec{B}$ is now considered the magnetic field flux density (T) and μ_o is the permeability of a vacuum (T m A^{-1}). The new parameters are identified as follows: μ, the magnetic permeability of the sample (T m A^{-1}); μ_r, the relative permeability of the sample (a.u.); and $\vec{H}$, the magnetic field induced in the sample (A m^{-1}). We must acknowledge that the relationship given by eq 8 is not intuitive for a few reasons, and there is a good deal of confusion surrounding the difference between the "$\vec{B}$ field" and the "$\vec{H}$ field". Both $\vec{B}$ and $\vec{H}$ represent a magnetic field strength and yet, they have different units in the SI system (in the older Gaussian Unit system, this problem is avoided as μ_o is defined to be 1 and dimensionless) and some textbooks/papers can use B and H interchangeably for calculating magnetic field strengths.[36] In this work, we have chosen to use "$\vec{B}$" as the symbol for the magnetic field strength calculated from Ampere's Law (eq 1) and the Biot–Savart Law (eq 3). This is partially due to historic reasons and a practical method to differentiate two magnetic fields interacting with

each other. This unfortunately makes the concept unclear when dealing with induction, as a magnetic field inside the sample is induced by an external magnetic field. Without going too deep into the mathematics, we can say that $\vec{H}$ is the magnetic field strength that is induced in the sample, and $\vec{B}$ is the resulting magnetic field experienced by the sample that is caused by the permeability (μ).[37] For many applications, it is suitable to assume that μ_r is equal to 1 and that the magnetic field is therefore proportional to the permeability in vacuum. The reason for this is that the relative permeability of many materials, including conductive metals, is very close to one. The main exceptions to this rule are ferromagnetic metals such as Ni, Co, and Fe, which have relative magnetic permeabilities of $\gg$1.[38] This implies that the induced field $\vec{H}$ within the material would be much greater than the applied field $\vec{B}$ to these materials.[36,37] The relative permeability (μ_r) is further related to the magnetization of the sample ($\vec{M}$) and is related to eq 8 through the following relationship:[35−37]

$$\vec{B}(\vec{r}) = \mu_o(\vec{H}(\vec{r}) + \vec{M}(\vec{r})) = \mu_o\vec{H}(\vec{r})(1 + \chi) = \mu_o\mu_r\vec{H}(\vec{r}) \tag{9}$$

where

$$\chi = \frac{\vec{M}(\vec{r})}{\vec{H}(\vec{r})} = \mu_r - 1$$

The new term ($\vec{M}$) is the magnetization of the sample (A m^{-1}) and χ is the volumetric magnetic susceptibility of the sample (a.u.) and is defined as the ratio between $\vec{M}$ and $\vec{H}$. Magnetization is related to ability of a sample to become magnetized by an external field, although it is common to omit this term, as $\vec{M}$ is 0 in a vacuum and often negligible in air, and the $\vec{H}$ field is often simply assumed to have a magnetization component. It follows from the previous discussion for eq 8 that paramagnetic materials tend to have slightly positive χ values and diamagnetic materials have slightly negative values, which results in deviations of μ_r from 1. Ferromagnetic materials do not have well-defined values of χ and, as a result, are often experimentally measured. This explains why μ_r for ferromagnetic materials can be $\gg$1. This has a significant impact on the penetration depth of the eddy currents into the sample. Alternating current has a tendency to accumulate within the surface region of conductors and the penetration is dependent on the intrinsic properties of the material and the inductor. This is known as the "skin effect", as the current is the densest near the material's surface and decays toward its bulk. The skin effect is summarized by the following relationship:[34]

$$I(d) = I_s e^{-d/\delta} \tag{10}$$

where $I(d)$ is the current at a given distance (depth) from the surface (A), I_s the current at the surface (A), d a distance (depth) from the surface (m), and δ the so-called "skin depth" (m). The skin depth is essentially the distance where the current decays to 1/e (ca. 37%) value, relative to the current at the surface. It is important to recognize that the skin depth varies, depending on the material as well as the inductor. A practical formula for the skin depth is given as follows:[33,35]

$$\delta = \sqrt{\frac{2\rho_R}{\omega\mu}} = \frac{1}{\sqrt{\pi f\sigma\mu}} \tag{11}$$

where ρ_R is the resistivity of a sample (Ω m), ω the angular frequency of the induction current ($2\pi f$, Hz), f the frequency of the induction current (Hz), σ the conductivity of the sample (S m^{-1}), and μ the magnetic permeability of a sample (H m^{-1} or N A^{-2}). A general rule of thumb is that the electrical resistance begins to become significant if the skin depth is thinner than the radius of the conductor.[35] The electrical resistance of a material is given by[39]

$$R = \rho_R\left(\frac{l}{A}\right) \tag{12}$$

where l is the length (m) and A is the area (m^2) of the sample.

THERMAL CONSIDERATIONS

In the previous section, we have explained that the resistance of a sample affects the extent to which a sample is heated. However, it is important to note that the resistance of a sample will change with temperature, according to the following relationship:[34]

$$R(T) = R_0[1 + \alpha_R(T - T_0)] \tag{14}$$

where $R(T)$ is the resistance (Ω) in the sample at a certain temperature T (K), R_0 the resistance (Ω) of the sample at a reference temperature T_0 (K), and α_R the temperature coefficient of resistance (K^{-1}). The value of α_R can be evaluated experimentally and is dependent on the physical properties of the material. The values of α_R have a tendency to be quite small, so within small temperature ranges or under close to ambient conditions, the effect is almost insignificant. However, if one is inductively heating a sample, and large temperature ranges are common, then it is important to consider the resistance change. The total amount of thermal energy required to raise the temperature of a sample is given by the following well-known equation:[39]

$$Q = mc_p\Delta T = \rho Vc_p\Delta T \tag{15}$$

where Q is the total amount of thermal energy (enthalpy, heat) being transferred (J), m the mass of the sample (kg), ρ the mass density of the sample (kg m^{-3}), V the volume of the sample (m^3), c_p the constant pressure specific heat capacity (J K^{-1} kg^{-1}), and ΔT the temperature difference (K). It is often more useful to think about the volume of a sample being heated, rather than a specific mass since the sample is being heated through an interaction of a magnetic field. The working distance and orientation of the sample will dictate the relative amount of exposure to the field, which is more closely aligned to the sample's volume rather than to its mass. When thinking in terms of sample volume, the density of the material is also introduced, which is intrinsic to each material, and implies that the denser the material, the more energy is required to heat it (in eq 15, the value of Q is proportional to the value of m). Therefore, how much of the sample is being exposed is dependent on the shape, as well as on the volume, of a sample. This connects with a correlation that we have discussed in the previous section about how the geometry of a sample affects the overall resistance of a sample. Materials have a tendency to expand as their temperature increases, according to the thermal expansion coefficient:[39]

$$\alpha_V = \frac{1}{V}\left(\frac{\partial V}{\partial T}\right)_p \tag{16}$$

where α_V is the thermal expansion coefficient of the sample (K^{-1}) and $\partial V/\partial T$ is the rate of change of the volume with temperature ($m^3\ K^{-1}$). Note that materials are also subject to volume changes if there is a significant pressure or vacuum placed upon them; this is referenced as the isothermal compressibility. However, for ambient conditions that are common for the heat treatments of samples for electrochemical measurements, pressure differences are often minimal and the volume change because of compression or relaxation of the sample is negligible.

In the previous section, we have shown that there is a tendency for the induced current to accumulate within the near-surface region of the sample and its penetration is governed by the skin effect. However, the thermal energy that this created via the Joule effect will propagate from the near-surface region of the sample to its bulk due to thermal conduction. The general expression for how heat propagates through a material is given by Fourier's Law of Heat Transfer:[40]

$$\vec{q} = -k\vec{\nabla}T = -k\left(\frac{\mathrm{d}T}{\mathrm{d}x}\vec{e}_x + \frac{\mathrm{d}T}{\mathrm{d}y}\vec{e}_y + \frac{\mathrm{d}T}{\mathrm{d}z}\vec{e}_z\right) \tag{17}$$

where $\vec{q}$ is the heat flux through the medium ($W\ m^{-2}$), k the thermal conductivity of a sample ($W\ m^{-1}\ K^{-1}$), and $\vec{\nabla}T$ is the temperature gradient of the medium ($K\ m^{-1}$). The negative sign in this equation implies that the heat is being transferred in the opposite direction of the temperature gradient. This is consistent with the Second Law of Thermodynamics, stating that the thermal energy flows from the high temperature region to the low temperature one.[39] This expression is a general one, where the heat is being transferred in all directions away from the heat source in the Cartesian coordinates. If the sample is comprised of a single material and is homogeneous (not composed of multiple phases or porous), then eq 17 can be simplified to the following expression:[40]

$$|\vec{q}| = -k\left(\frac{A}{l}\right)\Delta T \tag{18}$$

where A is the area of the sample (m^2), l is the thickness of the sample (m), and ΔT is the temperature difference (K). The simplified expression shows that heat is transferred as a result of a temperature difference (ΔT) within the sample and its magnitude increases as A increases and l decreases. This equation demonstrates, again, that the shape of the sample impacts how the sample is heated. The rate at which the sample is heated is defined by the thermal diffusivity:

$$\alpha_T = \frac{k}{\rho c_p} \tag{19}$$

where α_T is the thermal diffusivity of the medium ($m^2\ s^{-1}$). The thermal diffusivity is a ratio between the substance's ability to transfer heat (its thermal conductivity) to the ability of the substance to retain heat (density and specific heat capacity). This is an important consideration when comparing materials with similar thermal conductivities, as there could be significant differences in the rate at which energy is transferred. Like many physical properties of materials, thermal conductivity, density, and specific heat capacity change with temperature. For ambient conditions and over narrow temperature ranges, changes to these properties are often negligible. Over broad temperature ranges during thermal treatment, however, they can start to affect predicted values. Thus, it is important to consider these changes and remember that all three of these parameters have a tendency to change linearly with temperature. Thermal conductivities and densities have a tendency to decrease as the temperature increases, and the specific heat capacities have a tendency to increase. According to eq 19, this implies that thermal diffusivities will decrease with increasing temperature. The rates of change for these parameters are typically obtained experimentally, by linearly fitting measured data within a given temperature range at a constant pressure. However, it is important to note that changes of state (i.e., solid to liquid, liquid to gas, etc.) or phase transitions (depending on their direction, they absorb or released heat) can have profound impacts on these quantities, even if the temperature change is very small.

EMISSION OF LIGHT AND TEMPERATURE

All solid objects with a temperature above 0 K emit electromagnetic radiation and at elevated temperatures behave like blackbodies and emit electromagnetic radiation. Planck's Distribution Law (more commonly referred to as Planck's Law) relates the energy density of emitted photons to the temperature of the object and the wavelength of the emitted light:[41]

$$U_B(\lambda, T) = \frac{2hc^2}{\lambda^5}\left(\frac{1}{e^{hc/\lambda k_B T} - 1}\right) \tag{20}$$

where $U_B(\lambda,T)$ is the energy density of the emitted light of a blackbody ($J\ m^{-3}\ s^{-1}$), h Planck's constant (J s), c the speed of light ($m\ s^{-1}$), λ the wavelength of the light (m), k_B the Boltzmann constant ($J\ K^{-1}$), and T the temperature (K). The total intensity of photons produced by blackbody radiation is given by the Stefan–Boltzmann Law:[42]

$$I_B = \sigma T^4 \tag{21}$$

where I_B is the intensity of the emitted light of a blackbody ($J\ m^{-2}\ s^{-1}$), σ the Stefan–Boltzmann constant ($\sigma = 5.67 \times 10^{-8}\ J\ s^{-1}\ m^{-2}\ K^{-4}$), and T the temperature (K).

Planck's Law can be used to demonstrate the distribution of wavelengths of emitted photons by a solid object in relation to its temperatures (Figure 3). Because of a large difference in the intensity of the emitted photons at higher temperatures, which spans many orders of magnitude, the plots are normalized for a direct comparison of the distribution curves. However, it is

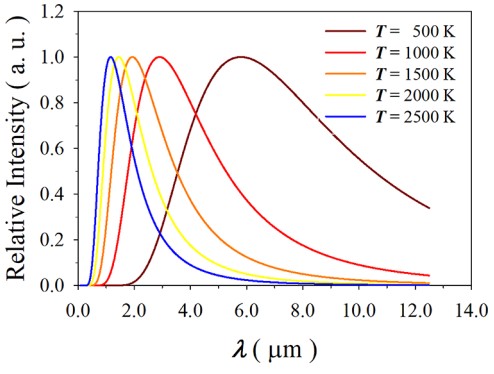

Figure 3. A series of plots showing the normalized photon intensity, with respect to the wavelength for a blackbody, according to Planck's Law for different temperatures.

important to mention that a hot object is much brighter than a cooler one and, as a result, the hot object will emit significantly more photons. The wavelength of the maximum in the Planck's Law distributions (λ_{max}), relative to the solid object's temperature, is referred to as Wien's Law:[41,43]

$$\lambda_{max} = \frac{2.898 \times 10^{-3} \text{m K}}{T} \quad (22)$$

where λ_{max} is the wavelength at maximum intensity (m) and T is the temperature (K). Wien's Law (eq 22) can be used to predict the temperature of a blackbody being at a given temperature T based on the peak wavelength, although it is more accurate to use the distribution described by Planck's Law (eq 20).[41,44] As can be observed from Figure 3, the energy distributions (i.e., wavelengths) of the radiation emitted by blackbodies are quite broad in a typical annealing temperature range, from 500 K to 2500 K, thus making it possible to determine the temperature of the analyzed solid based on the maximum amount of light that it emits. However, it is important to note that metals do not exactly behave like blackbodies. A blackbody is a theoretical object that absorbs 100% of the light that impinges on its surface, while emitting the maximum amount of light as a function of its temperature. Real materials, such as metals, will emit and absorb light at fraction of this theoretical maximum and are said to behave like "gray" bodies or imperfect emitters. This deviation arises from intrinsic properties of the material, as well as the nature of its surface. Kirchhoff's Law of Thermal Radiation (henceforth referred to as Kirchhoff's Law) assumes that, for a diffuse gray body emitter, the deviation from ideality is equal for both emission and absorption. We shall continue our discussion in terms of emission rather than absorption, but it is important to note that, because of Kirchhoff's Law, they are equivalent. This behavior is treated mathematically through the introduction of a new term, the emissivity (ε), which is a deviation factor that compares the total emission of photons of a real surface to that of a blackbody at the same temperature; the value of ε is in the 0−1 range. The assumption made by Kirchhoff's Law that deviations to emission and absorption are equal is a useful one, because it helps avoid thermodynamic paradoxes, e.g., if two bodies are in thermal exchange and one is at higher temperature but has lower emissivity, then it could appear that the hotter body could absorb thermal energy from the cooler one. Kirchhoff's Law prevents this because a body with a lower emissivity would also have lower absorptivity and be unable to absorb the radiation. Emissivity values are experimentally measured, because they are strongly dependent on the nature of the surface (i.e., surface morphology and roughness, degree of oxidation, shape, orientation toward the detector, etc.). They have a tendency to increase with temperature and can rapidly increase as a material melts. This is also the reason why solid/liquid interfaces can be readily identified optically.[45,46] Equations 19 and 20 can be modified for a real emitter by taking the emissivity into account:

$$U_{Real}(\lambda, T) = \varepsilon U_B(\lambda, T) \quad (23)$$

and

$$I_{Real} = \varepsilon I_B \quad (24)$$

where ε is the emissivity (a.u.), $U_{Real}(\lambda,T)$ and $U_B(\lambda,T)$ are the energy density of the emitted photons of a real surface and a blackbody, respectively (J m^{-3} s^{-1}), and I_{Real} and I_B are the intensities of the emitted light of a real surface and a blackbody, respectively (J m^{-2} s^{-1}). An important observation arises from an analysis of the energy distribution of emitted photons over a wide temperature range. As the temperature of the solid increases, more and more photons are emitted in the visible part of the spectrum (the intensity of at the maximum wavelength increases) and it becomes more visible to a detector. However, the human eye can only perceive certain colors when we observe a hot object and therefore the wavelengths of photons are not perceived uniquely or equally. Without going too deeply into the anatomy of the human eye, color perception is based on three types of light-detecting organs, called "cones", that detect red, green, and blue photons. As an object is heated and reaches a temperature of ∼600 °C, it begins to emit enough red photons to be detectable by the human eye. As the object's temperature is increased and is in the 800−1200 °C range, photons in the green part of the spectrum make the object appear orange to yellow. Increasing the object's temperature above 1300 °C, photons in the blue part of the spectrum are emitted and the object begins to appear white, as all of the color receptors in the human eye are being activated.[47] This phenomenon is referred to as "the color temperature" and for applications where accurate temperature values are not required or small temperature ranges are not analyzed, the object's temperature can be estimated alone by the color of light that is emitted. This approach is commonly used in flame annealing, where the description of object's temperature is given on a relative scale from red-, orange-, yellow-, to white-hot.[8] However, it is important to note that pictures taken of hot objects have a tendency to make them appear hotter than they really are, because the optics inside digital cameras have a tendency to be more sensitive and saturate faster than the human eye, making solid objects appear to be brighter and, consequently, hotter. This is an important observation that must be kept in mind if one tries to compare the color temperature of a photograph to the real color of a solid sample that is being heated.

PRACTICAL CONSIDERATIONS

We have shown in the previous sections that many variables affect how a sample behaves (how its temperature changes) during inductive heating. However, there are some very important, and possibly less obvious, practical, and experimental considerations that should be implemented to improve the quality of experiments and possibly prevent samples from being damaged during this thermal treatment. The following sections are some of the main observations and laboratory practices that have been identified for productive inductive heating for experimental research in electrocatalysis and interfacial electrochemistry.

SAMPLE POSITIONING

As it has been mentioned previously in the section entitled "Theory of Inductive Heating", the magnetic induction experienced by the sample is strongly dependent on its distance from the center of the induction coil. In the case of electrochemical applications that can lead to irreversible surface oxidation, structural transformation, or surface roughening, it may be necessary to heat-treat the sample repeatedly during a series of measurements to recover the same original surface arrangement of atoms. The sample must then be removed from an electrochemical cell in which experimental

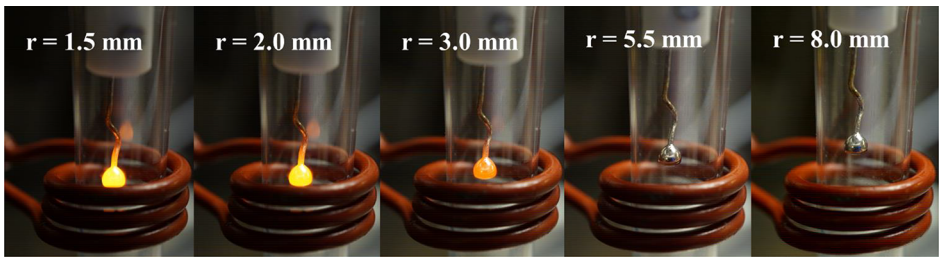

Figure 4. A series of images of a Ni(*hkl*) being heated at different distances *r* from the center of the induction coil. The flow of Ar(g) through the heating cell was 1.00 L min^{-1} and the induction heater was being operated at 120 A.

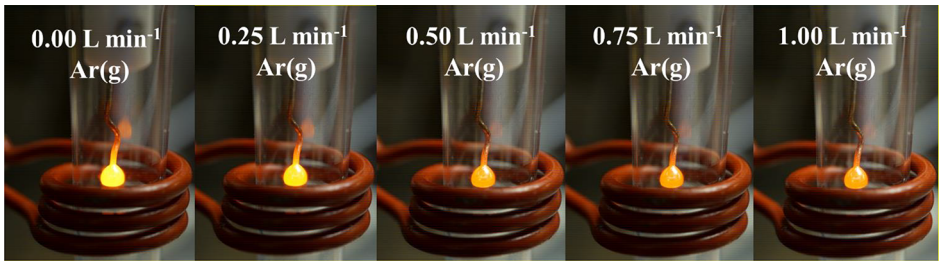

Figure 5. A series of images of a Ni(*hkl*) being heated with variable flow rates of gas flowing through the heating cell. The crystal was held at a distance of 2.0 mm from the center of the coil and the induction heater was being operated at 120 A.

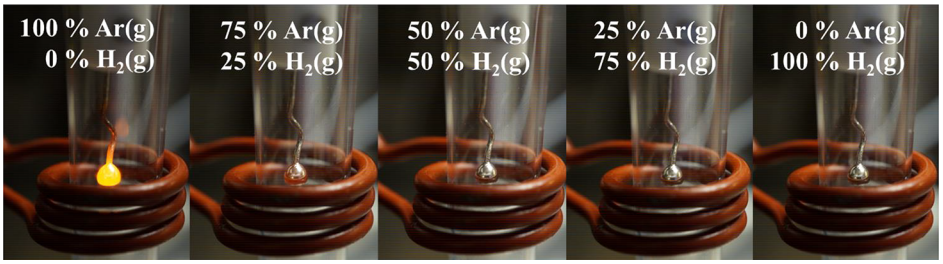

Figure 6. A series of images of a Ni(*hkl*) being heated with variable compositions of Ar(g) and H_2(g) flowing through the heating cell. The total flow rate of gas through the heating cell was 1.00 L min^{-1}, the crystal was held at a distance of 2.0 mm from the center of the coil and the induction heater was being operated at 120 A.

work is performed and returned to the induction heating setup for a new heat treatment. Such manipulations may result in slight variations in the distance between the sample and the center of the coil; thus, the same settings of the inductive annealing setup do not necessarily heat up the sample to exactly the same temperature. Figure 4 shows a series of images of a hemispherical Ni(*hkl*) being heated in an induction coil at varying vertical distances from the center of the coil. We have chosen to not start from the center of the coil (not from r_c = 0.0 mm) for clarity in viewing the Ni(*hkl*) sample. It is easily observed that the farther away the sample is placed from the center of the coil, the lower the temperature of the sample is for all other parameters being the same, in agreement with eq 5 and Figure 1. This practical observation is important as the effectiveness of the inductive heating may not be the same from one heat treatment to another even is all other settings are identical. In addition, if one is using an induction annealing setup in which the sample is vertically suspended, then it is essential to ensure that the sample position does not change during the duration of the heating. The glassware used in induction annealing systems is typically made of quartz or glass (see below) and they must be sealed from the surroundings in order to be able to maintain a predetermined and carefully controlled gaseous atmosphere on the inside. Gas seals for glassware are typically made of Viton or Teflon and, in a majority of electrochemical applications, are O-rings; they offer effective seals and can be cleaned using established procedures. However, if not regularly replaced with new, identical O-rings, they degrade, do not maintain the required seal, and can slightly affect the position of the sample inside the coil. Thus, it is essential to verify the structural integrity of the induction annealing system, and especially of its fragile components, on a regular basis.

GAS FLOW RATE AND COMPOSITION OF THE HEATING ATMOSPHERE

For many electrochemical and nonelectrochemical applications, where thermal treatment of a sample is required to obtain atomically ordered surfaces or oxide-free surfaces or to prevent the sample from being contaminated, it is often necessary to conduct the heating process in a controlled atmosphere. Figure 5 shows a series of images of the Ni(*hkl*) being heated at various flow rates of Ar(g). It is important to emphasize that, for the case of the flow rate of Ar(g) being 0.00 L min^{-1}, the Ni(*hkl*) sample is not being annealed in vacuum, as there is an ambient Ar(g) atmosphere present inside the annealing quartzware. In all cases, a thermal equilibrium is reached between the sample and the surroundings. Figure 5 shows that the temperature of the Ni(*hkl*) sample being heated gradually decreases as the Ar(g) flow rate increases from 0.25 L

min^{-1} and reaches the maximum flow rate of 1.00 L min^{-1}. An inspection of the images in Figure 5 might suggest that there is little temperature change as the Ar(g) flow rate is increased to 0.50 L min^{-1} and to 1.00 L min^{-1}. However, the temperature decrease is not significant enough to be perceptible via color change. This implies that a wide range of Ar(g) flow rates may be used as long as the gas flow rate does not exceed the maximum limit, because the sample temperature would be lower than the annealing temperature. However, from a practical point of view, it is experimentally simpler to work with lower than higher Ar(g) flow rates to preserve the integrity of seals, fittings, and joints of the annealing setup. Finally, in order to minimize any accidental and uncontrollable contaminating of samples, it is necessary to use UHP gases or gas mixtures when treating samples.

It is very common for electrochemists to employ gas mixtures when heat-treating or cooling monocrystalline electrodes.[8] This is typically done to create inert or slightly reducing atmospheres around the sample being heated, usually to thermally reduce oxides or to prevent them from reforming during the cooling step. Figure 6 shows a series of images of the Ni(*hkl*) being heated in mixtures of Ar(g) and H_2(g) of varying composition, as this is one of the most common gas mixtures used to treat monocrystalline surfaces of non-noble transition metals for electrochemistry and electrocatalysis measurements. It is immediately apparent from Figure 6 that increasing the relative amount of H_2(g) significantly reduces the temperature of the heated crystal (for all other variables being the same). This behavior is attributed to the thermal conductivity of H_2(g), which is about an order of magnitude higher than that of Ar(g) (186.6 mW m^{-1} K^{-1}, compared to 17.7 mW m^{-1} K^{-1} at 300 K, respectively).[48] Therefore, H_2(g) is much more efficient at conducting heat away from the crystal than Ar(g). This observation implies that a larger current must be passed through the coil to achieve the same temperature as the percentage of H_2(g) in the H_2(g)−Ar(g) mixture increases. Another important consequence of the thermal conductivity of gas mixtures is that the user must take special care to ensure that the flow rate of each of the mixture components remains constant throughout the heat treatment. This is especially relevant if the gases being used are part of a shared gas line system, because a sudden drop in the H_2(g) flow rate would cause a rapid temperature increase that may damage the sample being thermally treated. Thus, it is vital that flow meters or mass flow controllers are used to maintain a constant flow of each of the gas mixture components through the heating cell and that there is a sufficient quantity of gas available for the entire heat-treatment process, which can be lengthy.

DISCOLORATION OF GLASSWARE/QUARTZWARE

As previously mentioned, gas mixtures are often used to create slightly reducing atmospheres around heated samples. Most often, H_2(g) is used in combination with Ar(g) or N_2(g) to create slightly reducing atmospheres, but mixtures using CO(g) or CH_4(g) are also common. Quartz is an ideal material for the construction of a heating cell, since it is unaffected by the magnetic field around it, is transparent, is simple to clean, has a low value of the thermal expansion coefficient, and can maintain structural integrity at significantly higher temperatures than regular glasses. While quartz is unreactive at low temperatures, at higher temperatures, it can begin to react with reducing gases and become reduced. The exact reduction products are dependent on the reactive gas(es) and the temperature of the quartz.[49,50] The induction coil does not heat the quartz directly as previously mentioned, but radiation from the sample that is being heated can cause the quartz to heat up over time. Another important phenomenon that can occur is the spontaneous deposition of metallic species on the inner wall of the quartz over time. Many metals will slowly release atoms from their surfaces through sublimation while being heated as their vapor pressures become non-negligible at high temperatures.[48] In addition, if the sample is being heated in an atmosphere of CO(g) or there are organic contaminants that could lead to the formation of metallic carbonyls that are known to be very volatile (e.g., $Ni(CO)_4$), then the process will result in material loss. The thermal atomization (sublimation) of the metal and the exposure of its vapor to a cooler section of the annealing cell will result in the formation of a deposit that discolors and tints the quartzware. Similarly, decomposition of the metallic carbonyls will also cause metal to deposit on cooler parts of the quartzware, with a simultaneous release of CO(g). Again, this process will result in discoloration and tinting of the annealing cell over time.

Figure 7a shows a quartz annealing cell that has become discolored during the long heat treatment of a metallic crystal

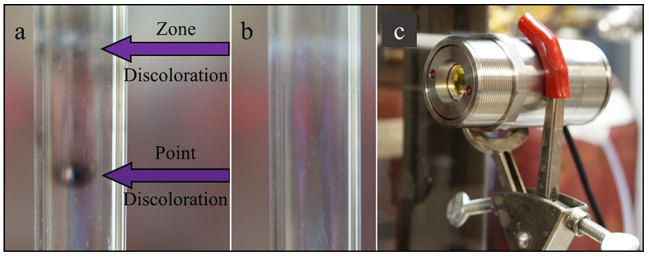

Figure 7. Images of a quartz annealing cell showing (a) discoloration and tinting of quartz tube caused by heating a sample in the presence of hydrogen gas across a zone and at a point; (b) the same quartz tube after being immersed in acidified $KMnO_4$ solution for 48 h; and (c) an IR laser pyrometer used for contactless temperature measurement.

in a slightly reducing atmosphere of Ar(g) and H_2(g). If a sample is large relative to the diameter of the quartz tube or if a sample is heated to particularly high temperatures, then an entire section or "zone" of the adjacent tube will become discolored. Smaller samples that are close to the wall of the quartz will likely not cause zone discolorations, but rather point discoloration, since only a small section of the quartz tube will heat up enough to become reduced. This also implies that the deposition of metallic species would also be more localized. Conveniently, the same solutions that are used by electrochemists to clean glassware for electrochemical measurements are often effective to remove discoloration from quartz.[29] Figure 7b shows the same quartz tube after being immersed in acidified $KMnO_4$ solution for 48 h. Depending on the extent of the discoloration, multiple-step cleaning treatments may be required to remove all the reduction products from the quartz. If discoloration persists, then it may be necessary to clean the quartzware with aqua regia (a 3:1 mixture of concentrated HCl(aq) and HNO_3(aq), respectively) to remove all metallic deposits through dissolution. However, the reduction of quartz can be more than an experimental nuisance. Induction heating systems do not inherently have temperature control ability, because of the wide range of factors that contribute to how a sample heats and

what the resulting temperature will be. To overcome this challenge, some manufacturers and researchers will couple pyrometers to their induction heating systems. This is often done when a specific temperature for heat treatment is required and routinely applied. Modern pyrometers often use lasers to properly align and orient the sample being heated; the measurement spot is the focal point of the guiding lasers, and its location is sensitive to both distance and orientation. The infrared radiation being emitted by the sample obeys the Stefan−Boltzmann Law and Kirchhoff's Law (it follows eqs 20 and 23) and is focused through lenses onto the detector inside the device. Thermopiles are often used as detectors that employ the thermoelectric effect to convert the measured thermal radiation into a small voltage that subsequently can be converted to a temperature reading.[51,52] Figure 7c shows a pyrometer that uses two infrared lasers to measure the sample's temperature. Based on the temperature reading, the induction heater can increase the applied current or power and thus can increase the sample's temperature. This is convenient because it allows for constant and contactless temperature measurement during heating. However, if the quartz begins to discolor, then the pyrometer can interpret this as the sample cooling as the detector can no longer effectively interact with the sample. This could cause overheating or potentially damaging the sample. If a coupled pyrometer-induction heater system is used, then it is imperative that the glassware/quartzware is regularly cleaned and any reduction products or deposits are removed. The extent of the reduction of the quartz can be minimized by reducing the amount of reducing gas(es) in the gas mixture for long heat treatments.

EXAMPLE ELECTROCHEMICAL RESULTS FOR NI(111)

In the previous section, we have demonstrated the principles of induction heating and discussed important practical considerations for optimal use of the technique. In this section, we will be using the cyclic voltammetry (CV) behavior of a Ni(111) electrode in 0.10 M aqueous NaOH as an example to show how induction annealing can be used to produce well-ordered, metallic surfaces for oxygen-sensitive metals and the effect of oxidation of the Ni(111) electrode on its CV behavior that is caused by exposure to oxygen from the air. It is well-known that metallic Ni is susceptible to oxidation when exposed to oxygen from the air, especially at elevated temperatures, which makes it essential that metallic Ni be isolated from oxygen during thermal treatment. While the controlled-atmosphere flame fusion (CAFF) methodology used to prepare polyoriented, spherical single crystals of Ni is described in detail elsewhere,[25] we will summarize the procedure in the following section to highlight the importance of isolating metallic Ni from oxygen to produce ordered surface structures. When Ni metal is heated to its melting point ($T_{m,Ni}$ = 1455 °C) in air, it will rapidly form an oxide layer of NiO that has a higher melting point ($T_{m,NiO}$ = 1955 °C) than metallic Ni, which results in sparking and material ejection as pressure builds under the oxide layer.[25,48] Proper crystal growth requires slow, controlled solidification of the metal, which is not possible if oxidation or material loss occurs. The CAFF methodology uses a custom-built chamber that isolates the molten Ni away from the air, by flowing a gentle stream of Ar(g) and using a H_2/O_2 flame with an excess of H_2(g) to produce a slightly reducing atmosphere. Under these conditions, high-quality, metallic Ni single crystals can be grown, and the growth process is an important demonstration of how oxidation can be prevented by isolating Ni from air and how ordered bulk and surface structures can form, even when it is being heated to high temperature. Furthermore, the notion that easily oxidizable transition metals can develop a surface oxide must be applied when performing electrochemical measurements on Ni(*hkl*) electrodes, since oxidation must be avoided in order to conduct measurements on a purely metallic surface (versus oxidized and possible disordered surfaces).

In aqueous alkaline media, a clean, metallic Ni surface will form α-Ni(OH)$_2$ when an anodic potential is applied in the $0.00 \leq E \leq 0.50$ V vs RHE range (all subsequent potential values are also reported, with respect to the RHE).[53] Reversing the direction of the potential scan will result in the reduction of the α-Ni(OH)$_2$ back to metallic Ni. The presence of these features is used as an indication that the Ni surface under study is metallic and oxide-free at the onset of experimentation. If the applied potential exceeds 0.50 V, then α-Ni(OH)$_2$ will covert to β-Ni(OH)$_2$ and form a passivating layer; the metallic state cannot be recovered without thermal treatment (reduction) in the presence of H_2(g) or through strong cathodic polarization.[54−56] A passive layer of β-Ni(OH)$_2$/NiO (NiO is the anhydrous form of β-Ni(OH)$_2$) will also form if metallic Ni is exposed to oxygen from the air prior to experimentation.[55] Thus, the presence of β-Ni(OH)$_2$ on the surface of the Ni electrode makes it impossible for α-Ni(OH)$_2$ to develop and to observe CV features associated with the process.[57] As discussed elsewhere, the CV profiles for monocrystalline metallic electrodes are unique to the nature of the metal, surface arrangement of atoms, and electrolyte composition and temperature, and serve as electrochemical "fingerprints".[25] Figure 8 shows three CV profiles of the Ni(111) electrode with

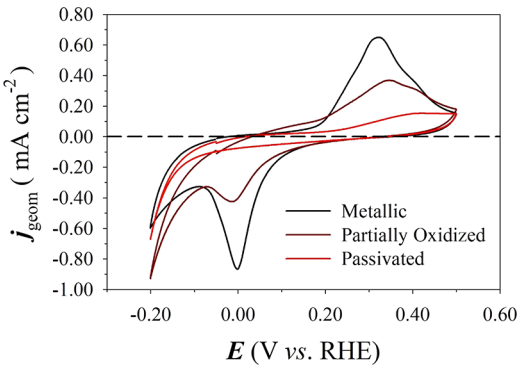

Figure 8. Cyclic voltammetry (CV) profiles of Ni(111) showing the effect of surface state on the CV behavior. The three transients refer to a metallic (black), partially oxidized (brown), and passivated (red) Ni(111) electrode. All transients were acquired in the -0.20 V $\leq E \leq$ 0.50 V range at a potential scan rate of s = 50 mV s^{-1} and a temperature of T = 298 K, and in 0.10 M aqueous NaOH solution.

varying degrees of surface oxidation. The black CV transient for a metallic (oxide-free) Ni(111) electrode shows prominent α-Ni(OH)$_2$ formation and reduction peaks at 0.33 and 0.00 V, respectively; these CV features and peak potentials of the Ni(111) electrode are consistent with our previous results.[25] The brown CV transient refers to a partially oxidized Ni(111) electrode and smaller features associated with the α-Ni(OH)$_2$ formation and reduction. In this instance, the transfer from the annealing cell to the electrochemical cell was deliberately

delayed for ca. 10 s, allowing oxygen from the air to diffuse into the protective water droplet (see the Experimental Section) and to partially oxidize the Ni(111) surface. It is apparent that the features associated with the formation and reduction of α-$Ni(OH)_2$ are present but suppressed compared to the metallic electrode. Lastly, the red CV transient refers to a passivated Ni(111) electrode, where after cooling in the $Ar(g)/H_2(g)$ atmosphere (see the Experimental Section) the Ni(111) electrode was transferred to the electrochemical cell without a protective water droplet, exposing the surface directly to oxygen from the air. It is readily observed that no features associated with the formation or reduction of α-$Ni(OH)_2$ are observed in this CV profile, demonstrating that the surface has been passivated by a layer of β-$Ni(OH)_2$/NiO. The suppression and distortion of the CV features associated with the formation and reduction of α-$Ni(OH)_2$ on a purely metallic Ni(111) serves as an important reminder that proper sample transfer from an annealing cell is just as important as proper heat treatment. The mechanisms, kinetics, and thermodynamics of electrochemical processes are incredibly dependent on the state of the electrode surface, and even slight surface oxidation can have profound impacts on the outcome of electrochemical measurements.[58,59] Although we present samples of results for a Ni(111) electrode to validate the method, elsewhere, similar results were reported for Ni(100) and Ni(110) electrodes.[25] Analogous results are needed for other non-noble transition metals and once produced will serve as important standards. The availability of CV transients for monocrystalline electrodes of non-noble transition metals in different aqueous electrolyte solutions (of different pH values and electrolyte compositions) will create a foundational knowledge that will advance atomic-level interfacial electrochemistry, electrocatalysis, and aqueous corrosion science.

CONCLUSIONS

The use of inductive heating in interfacial electrochemistry and electrocatalysis research has advanced the field and has allowed for measurements on the monocrystalline surfaces of non-noble transition metals that easily oxidize. With the invention of new and more complex methodologies for the preparation of high-quality metal, alloy, or thin-film deposits on single-crystal surfaces, there is an increasing demand for accurate thermal treatment procedures. In this contribution, we discuss the fundamental theory behind inductive heating. Starting from Ampere's Law, we describe how a current-carrying coil produces a magnetic field that interacts with a conductive sample. This interaction produces opposing eddy currents that cause the sample to heat (Joule effect). Magnetic and electric considerations including how materials will heat based on their inherent properties and how the induced current will be distributed throughout the sample are also discussed. The effect of sample shape and size and thermal considerations are examined, as well as how thermal energy is transferred through a sample, and how intrinsic properties of materials change with temperature. This section is concluded with a discussion of how heated samples emit radiation and how real samples (gray body emitters) compare with theoretical blackbody emitters. In the final section of this contribution, we discuss practical experimental considerations that offer important observations and recommendations to assist users to best utilize induction heating. The effects of flow rate and gas composition of common gaseous mixtures that are commonly used in the final preparation of surfaces for electrochemical measurements are demonstrated using hemispherical, Ni single crystals. Important experimental observations surrounding the maintenance of glassware/quartzware during inductive heating are discussed. Finally, we demonstrate the ability of induction annealing to produce well-ordered metallic surfaces and analyze the effect of oxygen contamination on the cyclic voltammetry features on a Ni(111) electrode in aqueous alkaline solution as an example. This provides an important reminder that, even with proper thermal treatment, proper sample handling and transfer from the annealing cell to the electrochemical cell is just as important to obtain good-quality electrochemical results. We believe that this contribution is a thorough and useful description of the use of induction heating for electrocatalysis research that will benefit not only electrochemists, but any researcher who would like to learn about or use this incredible technique.

AUTHOR INFORMATION

Corresponding Authors

Derek Esau − *Department of Chemistry, Queen's University, Kingston, Ontario K7L 3N6, Canada*; Email: 0dmce@queensu.ca

Gregory Jerkiewicz − *Department of Chemistry, Queen's University, Kingston, Ontario K7L 3N6, Canada*; orcid.org/0000-0003-1121-7291; Email: gregory.jerkiewicz@queensu.ca

Authors

Fabian M. Schuett − *Institute of Electrochemistry, Ulm University, 89069 Ulm, Germany*

K. Liam Varvaris − *Department of Chemistry, Queen's University, Kingston, Ontario K7L 3N6, Canada*

Ludwig A. Kibler − *Institute of Electrochemistry, Ulm University, 89069 Ulm, Germany*; orcid.org/0000-0003-1152-1445

Timo Jacob − *Institute of Electrochemistry, Ulm University, 89069 Ulm, Germany; Helmholtz-Institute-Ulm (HIU) Electrochemical Energy Storage, 89081 Ulm, Germany; Karlsruhe Institute of Technology (KIT), 76021 Karlsruhe, Germany*; orcid.org/0000-0001-7777-2306

Complete contact information is available at: https://pubs.acs.org/10.1021/acscatal.2c02174

Funding

This research was conducted as part of the Engineered Nickel Catalysts for Electrochemical Clean Energy project administered from Queen's University and supported by Grant No. RGPNM 477963-2015 under the Natural Sciences and Engineering Research Council of Canada (NSERC) Discovery Frontiers Program. This work was supported by MITACS through the Globalink Research Award and the DAAD which made the collaboration between Queen's University and Ulm University possible. This work was funded by the German Research Foundation (DFG) under Project ID No. 390874152 (POLiS Cluster of Excellence) as well as the Sonderforschungsbereich (Collaborative Research Center) No. SFB-1316.

Notes

The authors declare no competing financial interest.

■ ACKNOWLEDGMENTS

We gratefully acknowledge the technical support of Mr. Timothy Nash for producing the glassware/quartzware used in this contribution, as well as for helpful and insightful discussions about the properties of glass and quartz.

■ REFERENCES

(1) Jerkiewicz, G. Electrochemical Hydrogen Adsorption and Absorption. Part 1: Under-Potential Deposition of Hydrogen. *Electrocatalysis* **2010**, *1*, 179−199.
(2) Attard, G. A.; Price, R.; Al-Akl, A. Palladium Adsorption on Pt(111): A Combined Electrochemical and Ultra-High Vacuum Study. *Electrochim. Acta* **1994**, *39*, 1525−1530.
(3) Wadayama, T.; Todoroki, N.; Yamada, Y.; Sugawara, T.; Miyamoto, K.; Iijama, Y. Oxygen Reduction Reaction Activities of Ni/Pt(111) Model Catalysts Fabricated by Molecular Beam Epitaxy. *Electrochem. Commun.* **2010**, *12*, 1112−1115.
(4) Soriaga, M. P. Ultra-High Vacuum Techniques in the Study of Single-Crystal Electrode Surfaces. *Prog. Surf. Sci.* **1992**, *39*, 325−443.
(5) Landolt, D. Fundamental Aspects of Electropolishing. *Electrochim. Acta* **1987**, *32*, 1−11.
(6) Yang, G.; Wang, B.; Tawfiq, K.; Wei, H.; Zhou, S.; Chen, G. Electropolishing of Surfaces: Theory and Applications. *Surf. Eng.* **2017**, *33*, 149−166.
(7) Itaya, K. In Situ Scanning Tunneling Microscopy in Electrolyte Solutions. *Prog. Surf. Sci.* **1998**, *58*, 121−247.
(8) Kibler, L. A. Preparation and Characterization of Noble Metal Single Crystal Electrode Surfaces Preparation and Characterization of Noble Metal Single Crystal Electrode Surfaces. *Int. Soc. Electrochem.* **2003**, 1−56.
(9) Clavilier, J.; Faure, R.; Guinet, G.; Durand, R. Preparation of Monocrystalline Pt Microelectrodes and Electrochemical Study of the Plane Surfaces Cut in the Direction of the {111} and {110} Planes. *J. Electroanal. Chem.* **1980**, *107*, 205−209.
(10) Clavilier, J. The Role of Anion on the Electrochemical Behaviour of a {111} Platinum Surface; an Unusual Splitting of the Voltammogram in the Hydrogen Region. *J. Electroanal. Chem. Interfacial Electrochem.* **1980**, *107*, 211−216.
(11) Clavilier, J.; Armand, D.; Wu, B. L. Electrochemical Study of the Initial Surface Condition of Platinum Surfaces with (100) and (111) Orientations. *J. Electroanal. Chem.* **1982**, *135*, 159−166.
(12) Zurawski, D.; Rice, L.; Hourani, M.; Wieckowski, A. The In-Situ Preparation of Well-Defined, Single Crystal Electrodes. *J. Electroanal. Chem. Interfacial Electrochem.* **1987**, *230*, 221−231.
(13) Wang, K.; Chottiner, G. S.; Scherson, D. A. Electrochemistry of Nickel(111) in Alkaline Electrolytes. *J. Phys. Chem.* **1993**, *97*, 10108−10111.
(14) Cuesta, A.; Kibler, L. A.; Kolb, D. M. A Method to Prepare Single Crystal Electrodes of Reactive Metals: Application to Pd(hkl). *J. Electroanal. Chem.* **1999**, *466* (2), 165−168.
(15) El-Aziz, A. M.; Kibler, L. A. New Information about the Electrochemical Behaviour of Ru(0001) in Perchloric Acid Solutions. *Electrochem. Commun.* **2002**, *4*, 866−870.
(16) El-Aziz, A. M.; Kibler, L. A.; Kolb, D. M. The Potentials of Zero Charge of Pd(111) and Thin Pd Overlayers on Au(111). *Electrochem. Commun.* **2002**, *4*, 535−539.
(17) Schweizer, M.; Kolb, D. M. First Observation of an Ordered Sulfate Adlayer on Ag Single Crystal Electrodes. *Surf. Sci.* **2003**, *544*, 93−102.
(18) Pajkossy, T.; Kibler, L. A.; Kolb, D. M. Voltammetry and Impedance Measurements of Ir(111) Electrodes in Aqueous Solutions. *J. Electroanal. Chem.* **2005**, *582*, 69−75.
(19) Soliman, K. A.; Simeone, F. C.; Kibler, L. A. Electrochemical Behaviour of Nano-Faceted Ir(210). *Electrochem. Commun.* **2009**, *11*, 31−33.
(20) El-Aziz, A. M.; Hoyer, R.; Kibler, L. A. Preparation and Electrochemical Behavior of PtRu(111) Alloy Single-Crystal Surfaces. *ChemPhysChem* **2010**, *11*, 2906−2911.
(21) Heider, E. A.; Jacob, T.; Kibler, L. A. Platinum Overlayers on Pt_xRu_{1-x}(111) Electrodes: Tailoring the ORR Activity by Lateral Strain and Ligand Effects. *J. Electroanal. Chem.* **2018**, *819*, 289−295.
(22) Xu, Q.; Linke, U.; Bujak, R.; Wandlowski, T. Preparation and Electrochemical Characterization of Low-Index Rhodium Single Crystal Electrodes in Sulfuric Acid. *Electrochim. Acta* **2009**, *54*, 5509−5521.
(23) Özer, E.; Paul, B.; Spöri, C.; Strasser, P. Coupled Inductive Annealing-Electrochemical Setup for Controlled Preparation and Characterization of Alloy Crystal Surface Electrodes. *Small Methods* **2019**, *3*, 1800232.
(24) Bondarenko, A. S.; Stephens, I. E. L.; Bech, L.; Chorkendorff, I. Probing Adsorption Phenomena on a Single Crystal Pt-Alloy Surface under Oxygen Reduction Reaction Conditions. *Electrochim. Acta* **2012**, *82*, 517−523.
(25) Esau, D.; Schuett, F. M.; Varvaris, K. L.; Björk, J.; Jacob, T.; Jerkiewicz, G. Controlled-Atmosphere Flame Fusion Growth of Nickel Poly-Oriented Spherical Single Crystals—Unraveling Decades of Impossibility. *Electrocatalysis* **2020**, *11*, 1−13.
(26) Tymoczko, J.; Schuhmann, W.; Bandarenka, A. S. A Versatile Electrochemical Cell for the Preparation and Characterisation of Model Electrocatalytic Systems. *Phys. Chem. Chem. Phys.* **2013**, *15* (31), 12998−13004.
(27) Arulmozhi, N.; Jerkiewicz, G. Design and Development of Instrumentations for the Preparation of Platinum Single Crystals for Electrochemistry and Electrocatalysis Research. Part 1: Semi-Automated Crystal Growth. *Electrocatalysis* **2016**, *7*, 507−518.
(28) Arulmozhi, N.; Jerkiewicz, G. Design and Development of Instrumentations for the Preparation of Platinum Single Crystals for Electrochemistry and Electrocatalysis Research. Part 2: Orientation, Cutting, and Annealing. *Electrocatalysis* **2017**, *8*, 399−413.
(29) Arulmozhi, N.; Esau, D.; van Drunen, J.; Jerkiewicz, G. Design and Development of Instrumentations for the Preparation of Platinum Single Crystals for Electrochemistry and Electrocatalysis Research Part 3: Final Treatment, Electrochemical Measurements, and Recommended Laboratory Practices. *Electrocatalysis* **2018**, *9*, 113−123.
(30) Schuett, F. M.; Esau, D.; Varvaris, K. L.; Gelman, S.; Björk, J.; Rosen, J.; Jerkiewicz, G.; Jacob, T. Controlled-Atmosphere Flame Fusion Single-Crystal Growth of Non-Noble Fcc, Hcp, and Bcc Metals Using Copper, Cobalt, and Iron. *Angew. Chemie - Int. Ed.* **2020**, *59* (32), 13246−13252.
(31) Bird, M. A.; Goodwin, S. E.; Walsh, D. A. Best Practice for Evaluating Electrocatalysts for Hydrogen Economy. *ACS Appl. Mater. Interfaces* **2020**, *12*, 20500−20506.
(32) Jerkiewicz, G. On the Applicability of Platinum as a Counter Electrode Material in Electrocatalysis Research. *ACS Catal.* **2022**, *12*, 2661−2670.
(33) Fujimoto, M. *Physics of Classical Electromagnetism*; Springer: New York, 2007; pp 83−157.
(34) Rudnev, V.; Loveless, D.; Cook, R. L. *Handbook of Induction Heating*, Second Edition; CRC Press: Boca Raton, FL, 2002; pp 98−189.
(35) Lenaerts, B.; Puers, R. Omnidirectional Inductive Powering for Biomedical Implants. In *Omnidirectional Inductive Powering for Biomedical Implants*; Springer: Dordrecht, The Netherlands, 2009; pp 13−37.
(36) Bennett, L. H.; Page, C. H.; Swartzendruber, L. J. Comments on Units in Magnetism. *J. Res. Natl. Bur. Stand.* **1978**, *83*, 9−12.
(37) Wills, B., Finch, J. *Wills' Mineral Processing Technology—An Introduction to the Practical Aspects of Ore Treatment and Mineral Recovery*, 8th Edition; Elsevier: Oxford, U.K., 2016; pp 1−498.
(38) Belmans, R.; Hameyer, K. *Elektrische Energie: Fundamenten en Toepassingen*; Garant: Leuven, Belgium, 1999; pp 1−587.
(39) Atkins, P. W.; de Paula, J. *Physical Chemistry*, 9th Edition; W. H. Freeman: New York, 2010; pp 1−959.
(40) Sobota, T. Fourier's Law of Heat Conduction. In *Encyclopedia of Thermal Stresses*; Hetnarski, R. B., Ed.; Springer:Dordrecht, The Netherlands, 2014; pp 1769−1778.

(41) McQuarrie, D. A. *Quantum Chemistry*, 2nd Edition; University Science Books: Sausalito, CA, 2008; pp 1−683.
(42) Meseguer, J., Perez-Grande, I., Sanz-Andres, A. *Spacecraft Thermal Control*; Woodhead Publishing, Ltd.: Cambridge, U.K., 2012; pp 73−86.
(43) Ball, D. W. Wien's Displacement Law as a Function of Frequency. *J. Chem. Educ.* **2013**, *90*, 1250−1252.
(44) Overduin, J. M. Eyesight and the Solar Wien Peak. *Am. J. Phys.* **2003**, *71*, 216−219.
(45) Watanabe, H.; Susa, M.; Fukuyama, H.; Nagata, K. Phase (Liquid/Solid) Dependence of the Normal Spectral Emissivity for Iron, Cobalt, and Nickel at Melting Points. *Int. J. Thermophys.* **2003**, *24*, 473−488.
(46) Monier, R.; Thumerel, F.; Chapuis, J.; Soulié, F.; Bordreuil, C. Liquid Metals Surface Temperature Fields Measurements with a Two-Colour Pyrometer. *Meas. J. Int. Meas. Confed.* **2017**, *101*, 72−80.
(47) SECO Warwick. *Heat Treating Data Book*; SECO/Warwick: Meadville, PA, 2011; pp 1−107.
(48) *CRC Handbook of Chemistry and Physics*, 101st Edition; Rumble, J. R., Ed.; CRC Press/Taylor & Francis: Boca Raton, FL, 2020.
(49) McTaggart, F. K. Reduction of Silica in a Hydrogen Discharge. *Nature* **1964**, *201*, 1320−1321.
(50) Ksiazek, M.; Tangstad, M.; Dalaker, H.; Ringdalen, E. Reduction of SiO_2 to SiC Using Natural Gas. *Metall. Mater. Trans. E* **2014**, *1*, 272−279.
(51) Optris. Basic principles of non-contact temperature measurement. Available via the Internet at: https://www.optris.global/basic-principles-of-non-contact-temperature-measurement (accessed Jan. 27, 2022).
(52) Optris. Datasheet CTlaser 3M. Available via the Internet at: https://www.optris.global/optris-ctlaser-3m (accessed Jan. 27, 2022).
(53) Alsabet, M.; Grden, M.; Jerkiewicz, G. Electrochemical Growth of Surface Oxides on Nickel. Part 1: Formation of α-$Ni(OH)_2$ in Relation to the Polarization Potential, Polarization Time, and Temperature. *Electrocatalysis* **2011**, *2*, 317−330.
(54) Alsabet, M.; Grden, M.; Jerkiewicz, G. Electrochemical Growth of Surface Oxides on Nickel. Part 2: Formation of β-$Ni(OH)_2$ and NiO in Relation to the Polarization Potential, Polarization Time, and Temperature. *Electrocatalysis* **2014**, *5*, 136−147.
(55) van Drunen, J.; Kinkead, B.; Wang, M. C. P.; Sourty, E.; Gates, B. D.; Jerkiewicz, G. Comprehensive Structural, Surface-Chemical and Electrochemical Characterization of Nickel-Based Metallic Foams. *ACS Appl. Mater. Interfaces* **2013**, *5*, 6712−6722.
(56) Ferreira, E. B.; Jerkiewicz, G. On the Electrochemical Reduction of β-$Ni(OH)_2$ to Metallic Nickel. *Electrocatalysis* **2021**, *12*, 199−209.
(57) Grdeń, M.; Alsabet, M.; Jerkiewicz, G. Surface Science and Electrochemical Analysis of Nickel Foams. *ACS Appl. Mater. Interfaces* **2012**, *4*, 3012−3021.
(58) Oshchepkov, A. G.; Bonnefont, A.; Saveleva, V. A.; Papaefthimiou, V.; Zafeiratos, S.; Pronkin, S. N.; Parmon, V. N.; Savinova, E. R. Exploring the Influence of the Nickel Oxide Species on the Kinetics of Hydrogen Electrode Reactions in Alkaline Media. *Top. Catal.* **2016**, *59*, 1319−1331.
(59) Ferreira, E. B.; Tahmasebi, S.; Jerkiewicz, G. On the Catalytic Activity and Corrosion Behavior of Polycrystalline Nickel in Alkaline Media in the Presence of Neutral and Reactive Gases. *Electrocatalysis* **2021**, *12*, 146−164.